frontiers | Frontiers in Public Health

TYPE Original Research
PUBLISHED 07 December 2022
DOI 10.3389/fpubh.2022.970363

Check for updates

OPEN ACCESS

EDITED BY
Omar El Deeb,
Lebanese American University, Lebanon

REVIEWED BY
Saroj Kumar Chandra,
OP Jindal University Raigarh, India
Ayman Massaoudi,
Carthage University, Tunisia
Monika Yuliarti,
Sebelas Maret University, Indonesia

*CORRESPONDENCE
Jeffrey E. Harris
jeffrey@mit.edu

SPECIALTY SECTION
This article was submitted to Public Health Policy, a section of the journal Frontiers in Public Health

RECEIVED 15 June 2022
ACCEPTED 11 November 2022
PUBLISHED 07 December 2022

CITATION
Harris JE (2022) Concentric regulatory zones failed to halt surging COVID-19: Brooklyn 2020.
Front. Public Health 10:970363.
doi: 10.3389/fpubh.2022.970363

COPYRIGHT
© 2022 Harris. This is an open-access article distributed under the terms of the Creative Commons Attribution License (CC BY). The use, distribution or reproduction in other forums is permitted, provided the original author(s) and the copyright owner(s) are credited and that the original publication in this journal is cited, in accordance with accepted academic practice. No use, distribution or reproduction is permitted which does not comply with these terms.

Concentric regulatory zones failed to halt surging COVID-19: Brooklyn 2020

Jeffrey E. Harris[1,2]*

[1]Massachusetts Institute of Technology, Cambridge, MA, United States, [2]Eisner Health, Los Angeles, CA, United States

Methods: We relied on reports of confirmed case incidence and test positivity, along with data on the movements of devices with location-tracking software, to evaluate a novel scheme of three concentric regulatory zones introduced by then New York Governor Cuomo to address an outbreak of COVID-19 in South Brooklyn in the fall of 2020. The regulatory scheme imposed differential controls on access to eating places, schools, houses of worship, large gatherings and other businesses within the three zones, but without restrictions on mobility.

Results: Within the central red zone, COVID-19 incidence temporarily declined from 131.2 per 100,000 population during the week ending October 3 to 62.5 per 100,000 by the week ending October 31, but then rebounded to 153.6 per 100,000 by the week ending November 28. Within the intermediate orange and peripheral yellow zones combined, incidence steadily rose from 28.8 per 100,000 during the week ending October 3 to 109.9 per 100,000 by the week ending November 28. Data on device visits to pairs of eating establishments straddling the red-orange boundary confirmed compliance with access controls. More general analysis of device movements showed stable patterns of movement between and beyond zones unaffected by the Governor's orders. A geospatial regression model of COVID-19 incidence in relation to device movements across zip code tabulation areas identified a cluster of five high-movement ZCTAs with estimated reproduction number 1.91 (95% confidence interval, 1.27–2.55).

Discussion: In the highly populous area of South Brooklyn, controls on access alone, without restrictions on movement, were inadequate to halt an advancing COVID-19 outbreak.

KEYWORDS

SARS-CoV-2, mobility, mobile device tracking, geospatial regression, paired point-of-interest analysis

Introduction

The idea of drawing a series of concentric containment circles around an outbreak is well-established in the control of communicable diseases. The U.S. Department of Agriculture, for example, has adopted the model of three concentric containment zones – the infected zone, the buffer zone, and the surveillance zone – as its standard practice to contain highly contagious animal diseases (1). During the coronavirus disease 2019 (COVID-19) pandemic, the National

Task Force in the Philippines established a four-circle scheme to enforce graded degrees of quarantine: a critical zone subject to complete lockdown, where a cluster of cases had been identified; a surrounding 500-meter-radius containment zone where a modified lockdown prevailed; a surrounding buffer zone subject to community-level quarantine; and surrounding outside area with further relaxation of mobility controls (2, 3).

In their classic form, concentric regulatory zones have served as quarantine boundaries (4). Their use has been especially appealing when attack rates are directly related to the duration of contact and inversely related to the distance from an identifiable source, as they were in the Toronto-area severe acute respiratory syndrome (SARS) outbreak of 2003 (5). It is well-understood, however, that zone boundaries cannot simply be drawn around the areas of highest infection density, but need to take movement patterns into account (6).

On October 6, 2020, then New York Governor Cuomo issued a series of executive orders establishing a novel variation on the classic concentric control scheme (7). Rather than serving as mass quarantine boundaries, the concentric areas would define the extent of access control to restaurants, schools, gyms, houses of worship, and large gatherings generally. While several areas of concern were identified throughout the state of New York, far and away the principal challenge was the surge of new COVID-19 cases in the South Brooklyn area of New York City.

Our task here is to combine data on COVID-19 incidence and testing outcomes with data on the movements of devices equipped with location-tracking software to evaluate what happened over the ensuing months. Relying on geospatial regression analysis and spatial visualization tools (8), we find that the Governor's novel regulatory scheme failed to halt the surge of COVID-19. Our findings appear to go against the well-documented relationship between a reduction in mobility and a subsequent decline in COVID-19 incidence (9–14). To resolve the apparent contradiction, we distinguish between two types of mobility controls: regulations concerning access (15–17) and restrictions on movement (18–20).

Materials and methods

Regulatory background

By mid-September 2020, it had becoming increasingly evident that the recent surge of COVID-19 cases in certain hotspots of New York City was threatening the city's reopening plans. By September 29, then New York City Mayor de Blasio had signaled his intention to close non-essential businesses and all public and private schools in nine zip codes in the boroughs of Queens and Brooklyn for 14–28 days (21). The target zip codes included five in Brooklyn: Borough Park (11219), Gravesend (11223), Midwood (11230), Bensonhurst (11204), Flatlands (11210), and Gerritsen Beach/Homecrest/Sheepshead Bay (11229). Test positivity rates had increased beyond the acceptable threshold of 3% in these areas, exceeding 7% in Gravesend (11223) (22).

On October 6, however, then New York State Governor Cuomo intervened with his own regulatory control strategy, which he termed a "cluster action initiative" (7). Developed in consultation with public health experts, the initiative imposed new local restrictions on activity within "red zones" where clusters of new cases had been identified (23, 24). Recognizing that individuals within these high-risk areas tended to "interface with the surrounding communities," the initiative established two concentric rings – an intermediate orange zone and a peripheral yellow zone – surrounding the high-risk red zone.

Zone boundaries were drawn based on the test positivity rate, that is, confirmed COVID-19 cases as a percentage of all persons presenting for testing. Among highly populated areas, which included the borough of Brooklyn, a red zone was defined as having a sustained test positivity rate above 4 percent, while an orange zone had a rate from 3 to 4 percent, and a yellow zone had a rate from 2.5 to 3 percent (23).

Among the restrictions on activity, a red zone prohibited mass gatherings, allowed only essential businesses to open, closed in-person schooling, and restricted restaurants and other food providers to takeout/delivery only. An orange zone allowed gatherings up to 10 people, closed only high-risk businesses such as gyms and personal care, closed in-person schooling, and allowed outdoor dining with up to 4 persons per table. A yellow allowed gatherings up to 25 people, permitted all businesses to open, permitted indoor as well as outdoor dining up to four persons per table, and opened schools to in-person instruction subject to mandatory testing of students, teachers and staff (23). Restrictions on access to houses of worship were also initially imposed, with limits of 25% capacity in a red zone, 33% capacity in an orange zone, and 50% capacity in a yellow zone, but were subsequently blocked by the United States Supreme Court (25). The sanctions for failure to comply included withholding of funds to localities and schools (26).

Revisions of zone boundaries and changes in zone classification were based principally on the test positivity rate. On October 21, the Governor, citing the early success of the strategy in Brooklyn, reclassified the borough's original orange zone as a yellow zone, while the red zone remained unchanged (24). On November 3, citing further gains, the Governor reduced the size of the red zone by half (27). A few days later, on November 9, the red zone was reclassified as an orange zone (27), and subsequently as a yellow zone on November 18 (28). The zones were eventually dissolved without fanfare in January 2021.

Data sources: Regulatory zone boundaries

We determined regulatory zone boundaries from detailed maps issued by the office of the Governor of New

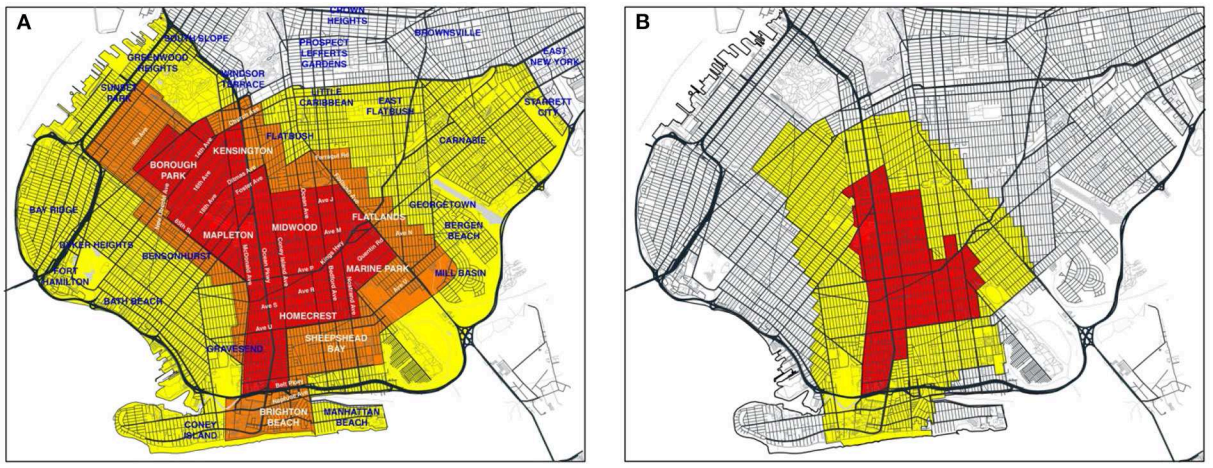

FIGURE 1
(A) Red, orange, and yellow zones effective October 9, 2020 (29), Overlaid on Annotated Map of South Brooklyn. On October 21, the orange zone was re-designated as a yellow zone, while the red zone remained unchanged (30). **(B)** Revised boundaries of red and yellow zones as of November 3 (32). On November 9, the red zone was re-designated as an orange zone (27), and subsequently as a yellow zone on November 18 (28).

York (29–31), along with accompanying announcements of updates (27, 28). Supplementary Figure A1 shows the boundaries of the original concentric red, orange, and yellow zones, effective October 9, 2020, overlaid on a street map of the larger New York City area (29). Figures 1A,B below depict the evolution of the regulatory zone boundaries, overlaid on more detailed street maps of South Brooklyn.

Figure 1A identifies the original red, orange and yellow zones (29). On October 21, the orange zone was incorporated into the existing yellow zone, while the original red zone boundaries remained unchanged (30). Figure 1B shows the contracted red and yellow zones as of November 3 (31). On November 9, the red zone was re-designated as an orange zone (27), and subsequently as a yellow zone on November 18 (28).

Data sources: Zip code tabulation area boundaries

Figures 2A,B superimpose the respective regulatory boundaries of Figures 1A,B on a map of zip code tabulation areas (ZCTAs) in South Brooklyn. The lack of complete congruence between the ZCTA and regulatory boundaries is evident. As discussed below, geographically detailed data on confirmed COVID-19 incidence over time was available only at the ZCTA level. Accordingly, for the purposes of analyzing COVID-19 incidence, we classified any of the nine ZCTAs that even partially overlapped the original red zone as an original red-zone ZCTA. These ZCTAs, indicated in boldface in Figure 2A, included 11204, 11210, 11218, 11219, 11223, 11229, 11230, 11234, and 11235. The remaining 12 ZCTAs, indicated in italics, were classified as original orange-yellow zone ZCTAs. In Figure 2B, the same classification of ZCTAs is shown in the map of the contracted regulatory zones effective November 3.

Data sources: Census block groups

As discussed below, we relied on the Safegraph Social Distancing database (34) to gauge the movements of devices equipped with location-tracking software throughout the greater New York City area. The origin and destination of each device movement in the Social Distancing database are keyed to census block groups (CBGs). Accordingly, we developed a separate correspondence between CBGs and regulatory zones, as shown in Figure 3A. Relying on Quantum Open Source Geographic Information System (QGIS) software (35), we determined the geocoordinates the centroids of all CBGs in South Brooklyn based upon their U.S. Census-defined shape files (36). Using the Stata Statistical Software (Stata) routine *geoinpoly* (37), we then assigned each CBG to the regulatory zone polygon in which its centroid was situated. While not explicitly shown in the figure, we used the same procedure to map CBGs into the ZCTA polygons shown in Figures 2A,B.

Data sources: Points of interest

We relied upon the SafeGraph Patterns database (38) – a source distinct from the Social Distancing database (34) – to analyze visits of devices to points of interest (POIs) within

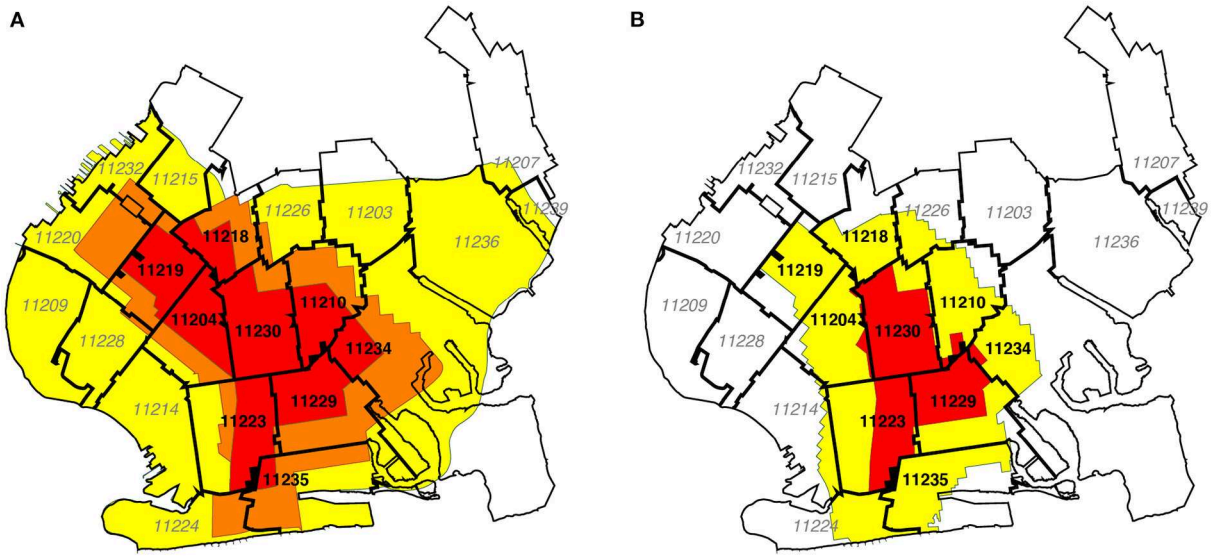

FIGURE 2
(A) Boundaries of the original October 9 zones overlaid on map of zip code tabulation areas (ZCTAs). In our calculations of confirmed COVID-19 incidence rates and test positivity rates, we assigned the nine ZCTAs in black boldface to the original red zone, while the remaining 12 ZCTAs in gray italic were assigned to the combined orange and yellow zones. **(B)** Updated boundaries of the redrawn November 3 zones overlaid on the same ZCTA Map. For base map of New York City ZCTAs, see Ref. (33).

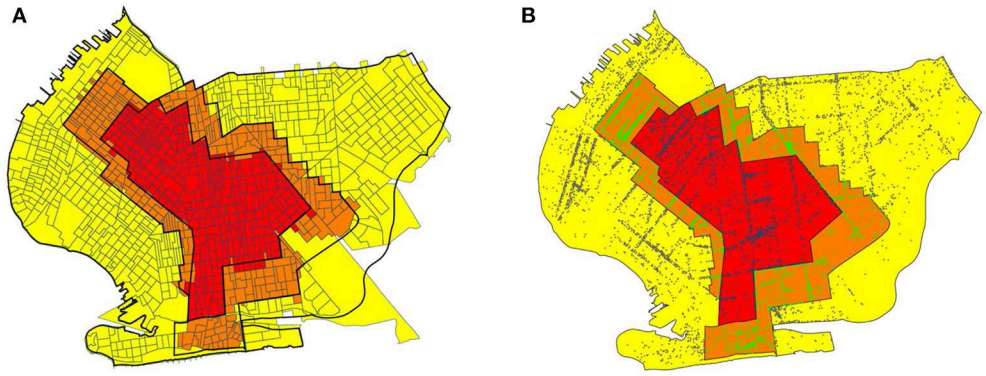

FIGURE 3
(A) Boundaries of the original October 9 zones overlaid on map of census block groups (CBGs). In our calculations of within- and between-zone device movements, we assigned each CBG to the zone containing its geographic centroid. **(B)** Boundaries of the original October 9 zones overlaid on map of Safegraph points of interest (POIs) (38). Each point corresponds to a POI. Points have different colors depending on the regulatory zone in which they were located. For base map of New York City census block groups, see Ref. (39).

the regulated area in South Brooklyn. At the broadest level, Safegraph classifies POIs according to the variable *top_category*, which includes such categories as "Automotive Repair and Maintenance," "Child Day Care Services," "Clothing Stores," "Elementary and Seconday Schools," "Gasoline Stations," and "Health and Personal Care Stores." One of the largest such categories is "Restaurants and Other Eating Places." Taking advantage of the Safegraph-supplied geocoordinates of each POI, and again relying on the Stata *geoinpoly* routine (37), we classified each POI as being located in one of the original three regulatory zones. Based upon this classification, we constructed Figure 3B, which plots the location of every POI as a color-coded point within the original October 9 regulated area.

Data sources: COVID-19 incidence and test positivity

We relied upon data published by the New York City Department of Health on COVID-19 incidence, measured as the number of confirmed cases per 100,000 population, and COVID-19 test positivity, measured as the percentage of positive

tests, broken down by ZCTA and week (40, 41). Both data sources covered the weeks ending August 8 through November 28, 2020.

Statistical methods: Paired point-of-interest analysis

We developed a paired point-of-interest (POI) analysis to test whether the regulations imposed by the Governor were in fact enforced and effective. To that end, we focused on device movements into restaurants and other eating places located in the original red zone, where establishments were restricted to takeout/delivery only, and in the original orange zone, where establishments could also offer outdoor dining with up to four persons per table (23). To avoid potentially biased comparisons between local dining patterns in distinct neighborhoods (such as Borough Park in the original red zone and Brighton Beach in the original orange zone, as shown in Figure 1A), we restricted our comparisons to pairs of nearby eating establishments that straddled the original red-orange border.

We identified all POIs in the SafeGraph Patterns database (38) with a *top_category* designated as "Restaurants and Other Eating Places." Within this restricted dataset, there were 395 POIs in the original red zone and 507 POIs in the original orange zone. (There were also 1,045 POIs in the original yellow zone, but they were not included in our paired POI analysis). Relying on the Stata program *geonear* (42), we isolated 219 pairs of red-zone and orange-zone POIs that were nearest neighbors of each other, where the maximum distance between POIs within each pair was 300 meters. The median distance between paired POIs was 130.9 meters, with 25th and 75th percentiles equal to 70.7 and 218.6 meters, respectively. Because a POI on one side of the red-orange boundary could be the nearest neighbor of multiple POIs on the other side, the resulting dataset contained 145 unique red-zone POIs and 114 unique orange-zone POIs. Supplementary Figure A2 maps two such pairs straddling the red-orange boundary running along Avenue U in Brooklyn.

Let I denote the set of all red-zone POIs, with typical element $i \in I$, and let J denote the set of all orange-zone POIs, with typical element $j \in J$. Then our database consists of a subset of 219 unique pairs (i, j) contained within the larger set $I \times J$. For each POI, we relied on the Safegraph Patterns variable *visits_by_day* to compute the number of visits during each week, starting with the week ending October 1 (designated $t = 0$) and continuing through the week ending December 3 ($t = 9$). We thus had 219 paired observations (y_{Rit}, y_{Ojt}), where y_{Rit} represents the number of visits during week t to red-zone POI i, and where y_{Ojt} represents the number of visits during week t to orange-zone POI j.

Given these data, we ran the following fixed-effects regression model:

$$\log\left(\frac{y_{Rit}}{y_{Ojt}}\right) = \mu + \beta_t + \theta_i + \phi_j + \epsilon_{ijt} \quad (1)$$

In equation (1), the parameter μ is an overall constant term, β_t, θ_i. and ϕ_j are fixed-effect parameters corresponding to each week t, red-zone POI i, and orange-zone POI j, and ϵ_{ijt} are independently distributed spherical error terms. Within this fixed-effects framework, only the contrasts $\beta_t - \beta_0$ ($t = 1,\ldots,9$) can be identified. If the regulations imposed by the Governor were in fact enforced and effective, then we would expect the estimated parameters β_t to be negative.

Statistical methods: Geospatial analysis

Movements to specific points of interest such as restaurants, auto repair shops and daycare centers are part of a larger set of movements to destinations that include private residences and workplaces. We sought to determine how these more general movement patterns related to the evolution of COVID-19 incidence, particularly during the period from the second half of October to the end of November, when cases of the disease were increasing throughout the regulated area in South Brooklyn. To that end, we developed a geospatial model relating COVID-19 incidence to general device movements. The central feature of this model was that the incidence of the disease in a particular ZCTA during a particular week was related to the incidence in all ZCTAs during the prior week. Moreover, the influence of one ZCTA on another was determined by the volume of device traffic between the two. The details of our model and its implementation are given in Appendix B.

Our model relied on two types of data: COVID-19 incidence and device movements. Because our data on COVID-19 incidence were based upon ZCTAs, we classified device movements between ZCTAs as well. Relying on data published by the New York City Department of Health (40), we constructed a data series $\{y_{kt}\}$ of the incidence of confirmed COVID-19 cases per 100,000 population in ZCTA k during week t, where $k = 1,\ldots,21$ indexes the 21 ZCTAs within the regulated area in Figure 2, and where $t = 1,\ldots,7$ indexes the 7-week period running from the week ending October 17 through the week ending November 28. Relying upon the variables *origin_census_block_group* and *destination_cbgs* in the Safegraph Social Distancing database (34), we constructed a data series $\{n_{k\ell t}\}$ of counts of device movements from ZCTA k into ZCTA ℓ during week t. The counts n_{kkt}, which represented the number of device movements staying within ZCTA k during week t, included those devices homed the ZCTA that made no movements. While we also observed device movements beyond the 21-ZCTA regulated area, as well as movements into the

regulated area from outside, we focused sharply on the regulated area in order to ascertain how the traffic between local ZCTAs influenced the dynamics of COVID-19 transmission.

Based upon our underlying data on device movements, we let V_t be a 21×21 square matrix with typical element $v_{k\ell t}$ measuring the proportion of all devices originating in ZCTA k that moved into ZCTA ℓ during week t. The elements of each row of V_t sum to 1. Likewise referring to week t, we let W_t be a 21×21 square matrix with typical element $w_{k\ell t}$ measuring the fraction of all devices with a destination in ZCTA ℓ that originated in ZCTA k. The elements of each column of W_t sum to 1. Let Y_t denote a 21×1 column vector with elements y_{kt}. We let Y_{t+1} represent the corresponding vector of incidence rates 1 week later, while η_{t+1} is a contemporaneous vector of error terms. Under the strong assumption of *homogeneous mixing*, our geospatial model yields:

$$Y_{t+1} = \alpha\ V_t\ W_t'\ Y_t + \eta_{t+1} \tag{2}$$

The model of equation (2) is an adaptation of the conventional law of mass action implicit in SIR-type compartmental models of the dynamics of contagious disease transmission (43). It allows for a susceptible individual homed in ZCTA k to be infected not only through contact with another resident of the same ZCTA k, but also through contact with a resident of another ZCTA ℓ. The inclusion of both vectors V_t and W_t, moreover, allows for two loci of transmission from an infected individual residing in ZCTA ℓ to a susceptible individual homed in ZCTA k. Either the susceptible individual homed in k had temporarily moved to ℓ, or the infected individual in ℓ had temporarily moved to k. The unknown parameter α in equation (2), to be estimated from the data, represents the uniform reproductive number for COVID-19 transmission throughout the entire regulated area for the 7-week time period under study.

Inhomogeneous mixing

The assumption of homogeneous mixing, with a uniform reproductive number α, is strong. Accordingly, we considered two alternative specifications involving inhomogeneous mixing. First, we assumed instead that movements by individuals who remained within their home ZCTA could have a different influence on COVID incidence. To capture the effect of these within-ZCTA device movements, we defined $D_t = \text{diag}\left(V_t W_t'\right)$ as the $K \times K$ square matrix with the same diagonal elements as $V_t W_t'$ but zero off-diagonal elements, and then introduced the additional regressor $D_t Y_t$ into our model. Defining the $K \times K$ square matrix $X_t = V_t W_t' - D_t$, we have:

$$Y_{t+1} = \alpha_0\ D_t\ Y_t + \alpha_1 X_t Y_L + \eta_{t+1} \tag{3}$$

We refer to this alternative as *inhomogeneous mixing model A*. In equation (3), the parameter α_0 reflects the reproductive number for within-ZCTA movements, while the parameter α_1 reflects the corresponding reproductive number for between-ZCTA movements. We estimated the models of equation (2) with weighted least squares, where the weights were the ZCTA populations derived from the New York City Department of Health data (40).

Second, we relaxed the assumption that all between-ZCTA movements had the same reproductive number α_1. Instead, movements to and from certain high-risk ZCTAs were permitted to exert more influence than movements to and from the remaining lower-risk ZCTAs. To capture such differences in transmission efficiency, we partitioned the set of ZCTAs into two mutually exclusive subsets, L and H, representing the low- and high-transmission ZCTAs, respectively. Conformally partitioning X_t vertically into two matrices, X_{tL} and X_{tH}, and the column vector Y_t horizontally into two vectors: Y_{tL} and Y_{tH}, our equation (3) becomes:

$$Y_{t+1} = \alpha_0\ D_t\ Y_t + \alpha_1 X_{tL} Y_{tL} + \alpha_2 X_{tH} Y_{tH} + \eta_{t+1} \tag{4}$$

The unknown parameters α_0, α_1, and α_2, respectively, represent the reproductive numbers for movements within-ZCTAs, movements to and from low-risk ZCTAs, and movements to and from high-risk ZCTAs. We refer to this alternative as *inhomogeneous mixing model B*.

We performed two tests of inhomogeneous mixing model B, based upon two different partitions of the set of 21 ZCTAs delineated in Figure 2. First, on the basis of our examination of the trends in inter-ZCTA movements, as detailed in the Results section, we identified five high-movement ZCTAs along the southern boundary of the 21-ZCTA area as the most likely elements of the high-risk set H. The estimates based upon this high-low partitioning of ZCTAs were identified as B1. Second, we relied on the original classification of regulatory zones specified in the Governor's order of October 6, with the red-zone ZCTAs specified as high risk (H) and the remaining orange and yellow zones specified as low risk (L). These estimates were identified as B2. We similarly estimated the inhomogeneous geospatial models of Equations (3) and (4) with population-weighted least squares.

The model of equations (1) through (4) does not account for potential confounding factors. In Appendix B, we show how the model can be extended to incorporate such potential confounders, and we test the effects of including three demographic characteristics as covariates: the proportion of persons of Hispanic-Latino origin; the proportion of black non-Hispanics; and the proportion of persons receiving public assistance. While mobile device use has become pervasive in the U.S., the lower rates of smartphone use among the poorest individuals (44), as well as racial and ethnic differences in the patterns of smartphone use (45), could have biased our results.

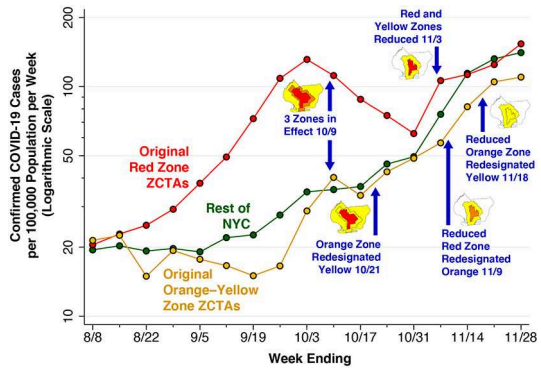

FIGURE 4
Confirmed COVID-19 cases per 100,000 population in the original red zone, original combined orange-yellow zones, and the rest of New York City, weeks ending 8/8 through 11/28/2020. The data points represent population-weighted rates, derived from ZCTA-specific weekly COVID-19 incidence as reported by the NYC Department of Health (40), and aggregated according to the scheme in Figure 2A. Superimposed on the graphic are the dates of five successive regulatory actions: (i) establishment of the original three zones on October 9 (7, 29); (ii) re-designation of the original orange zone as yellow on October 21 (24); (iii) reduction in the size of the red and orange zones on November 3 (27, 32); (iv) re-designation of the reduced red zone as orange on November 9 (27); and (v) re-designation of the reduced orange zone as yellow on November 18 (28).

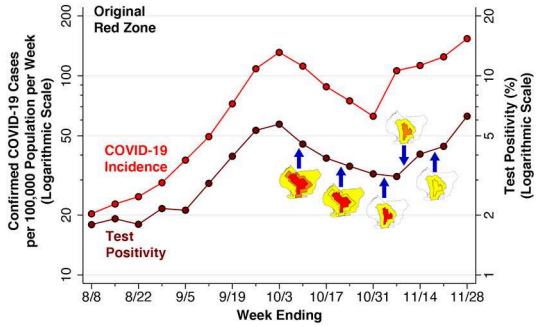

FIGURE 5
Confirmed COVID-19 cases per 100,000 population (Left Axis) and Test Positivity rate (Right Axis) in the Original Red Zone, weeks ending 8/8 through 11/28/2020. As in Figure 4, the data points represent population-weighted rates, derived from ZCTA-specific weekly COVID-19 incidence (40) and test positivity (41) among the ZCTAs identified as covering the red zone in Figure 2A. As in Figure 4, the blue arrows show the dates on which the five successive regulatory actions went into effect, while the accompanying maps show the corresponding zone changes.

Results

COVID-19 incidence and test positivity

Figure 4 below plots the incidence of confirmed cases of COVID-19 per 100,000 population in the original red zone, the original combined orange and yellow zones, and in the rest of New York City during the weeks ending August 8 through November 28. Also noted in the plot are the dates of Governor's five successive regulatory actions, starting with the imposition of the original three concentric zones, effective October 9. While the regulatory zones underwent revisions, the geographic areas used to compute case incidence in Figure 4 remained unchanged.

After rising during August and September, COVID-19 incidence in the ZCTAs comprising the original red zone started to decline during the week ending October 10, a time period that included 5 days before the regulatory scheme took effective. COVID-19 incidence in the red zone continued to decline through the week ending October 31, but then began to rebound. By contrast, COVID-19 incidence in the original orange and yellow zones, as well as the rest of New York City, had been increasing since at least mid-September, and reached approximately the same level as the original red zone by November. By November 21, all three series had exceeded the threshold of 100 cases per 100,000 population per week.

Figure 5 focuses sharply on the original red zone. The incidence of confirmed COVID-19 cases per 100,000 population, measured on the left-hand vertical scale, is reproduced from Figure 4. Superimposed on this time series is the test positivity rate, measured on the right-hand vertical scale. As in Figure 4, the dates when each of the five successive regulatory actions went into effect are noted. Again, while the regulatory zones underwent successive revisions, the geographic area used to compute the positivity rate – namely the original red zone – remained unchanged.

The variable vertical gap between the two time series in Figure 5 corresponds to the changing testing rate for COVID-19. Thus, the testing rate per 1,000 population progressively increased from 11.33 during the week ending August 8 to 17.15 during the week ending September 12, and then further increased to 24.61 by the week ending October 10. By the weeks ending November 7, 14 and 21, respectively, the testing rates had reached 33.99, 27.88, and 28.20 per 1,000 population.

Because the red-zone ZCTAs in Figure 2A only approximate the precise boundaries of the original red zone, the estimated test positivity rates plotted in Figure 5 represent only approximations to the positivity rates that were relied upon by state regulators. Still, during the week ending November 7, there is a striking divergence between the declining test positivity rate and the concurrently rising incidence rate. This finding suggests that regulators, relying on the trend in a test positivity rate that

was biased downward by enhanced testing, relaxed restrictions when in fact the incidence of the disease was rising.

Figure 6 below tracks the detailed evolution of COVID-19 incidence in each of the 21 ZCTAs identified in Figure 2 during the weeks ending September 12 through November 28. The first row, covering the weeks ending September 12 through October 3, shows increasing disease incidence in the central ZCTAs covering what would ultimately be designated as the red zone. In the second row, covering the weeks ending October 10 – 31, the incidence of COVID-19 was declining in the central ZCTAs but increasing in the peripheral ZCTAs, particularly along the southern and western borders of the South Brooklyn region. In the third row, covering the weeks ending November 7 – 28, COVID-19 incidence continued to rise in these peripheral ZCTAs, while resuming its upward trend in the central ZCTAs. By November 28, the original central zone of high-incidence ZCTAs is no longer distinguishable.

Visits to restaurants: Paired POI analysis

Figure 7 below shows the results of our paired POI analysis of visits to restaurants and other eating places. The estimate of $\beta_1 = -0.075$ for the week ending October 8 is negative and significantly different from zero in a two-sided test ($p = 0.0497$). That is, visits to restaurants in the red zone had already declined by 7.5% relative to those in the orange zone during the week before the regulatory scheme went into effect. While the individual estimates of $\beta_2 = -0.059$ and $\beta_3 = -0.067$ are not significantly different from zero, the overall downward trend is evident by the weeks ending October 29 and November 5, where $\beta_4 = -0.114$ ($p = 0.003$) and $\beta_5 = -0.172$ ($p < 0.001$). Thereafter, as the red zone is reduced by half (effective November 3), then reclassified as orange (effective November 9), and then reclassified as yellow (November 18), the estimates of β_t begin to rebound. By the week ending December 3, the

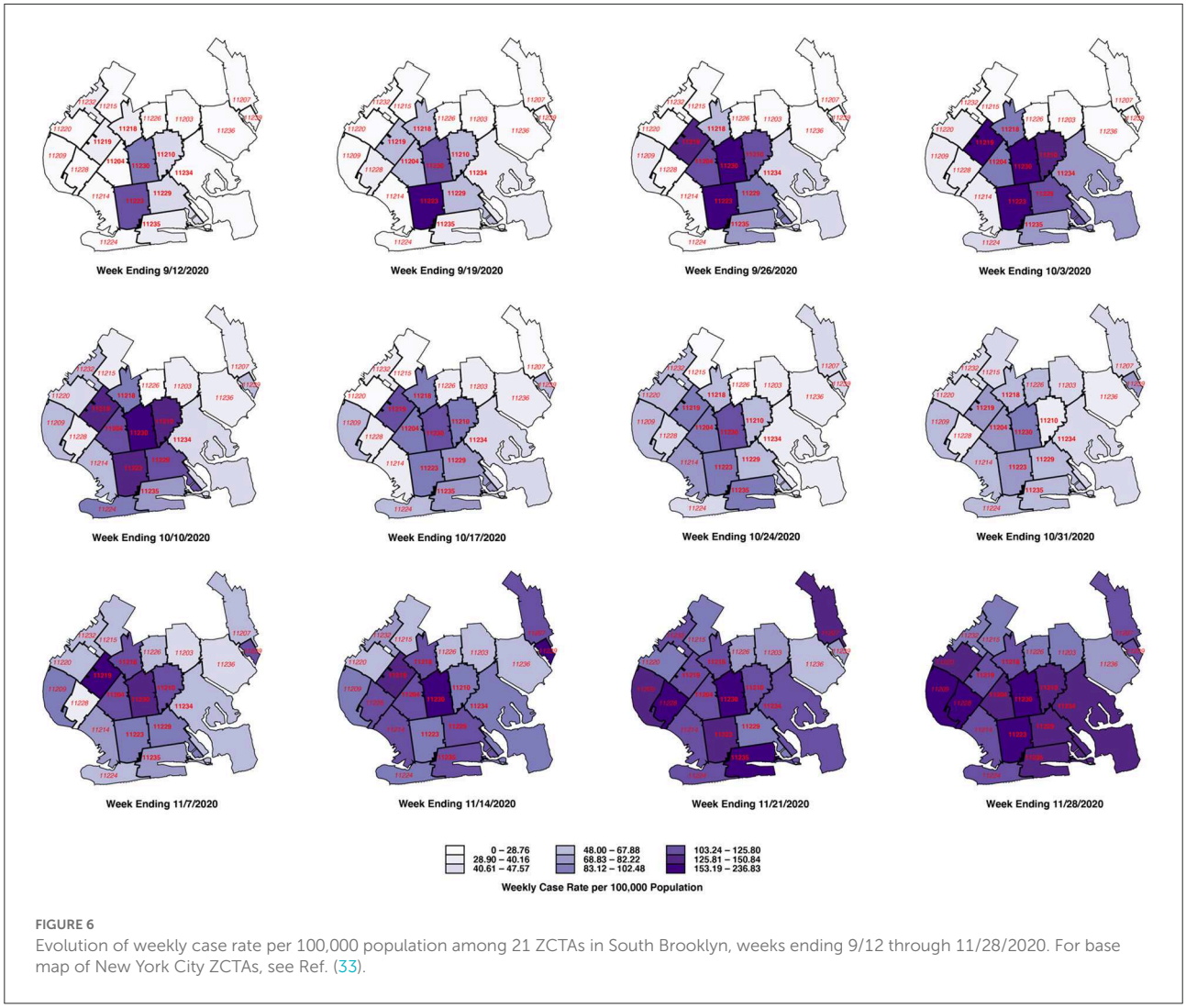

FIGURE 6
Evolution of weekly case rate per 100,000 population among 21 ZCTAs in South Brooklyn, weeks ending 9/12 through 11/28/2020. For base map of New York City ZCTAs, see Ref. (33).

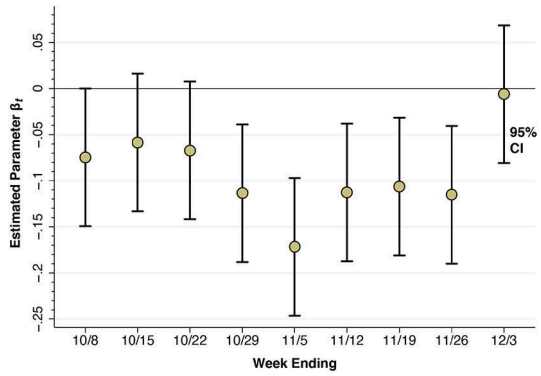

FIGURE 7
Estimated time-specific fixed effects derived from the paired point-of-interest analysis. Each point represents an estimate of the contrast $\beta_t - \beta_0$ for $t = 1,..., 9$, where $t = 0$ represents the week ending 10/1/20 as a reference category. The error bars surrounding each point represent 95% confidence intervals.

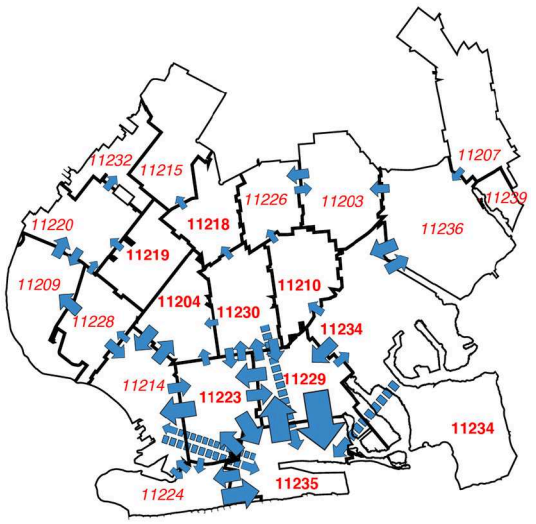

FIGURE 8
Most frequent transits between ZCTAs during 10/25 through 11/28/2020. The width of each blue arrow is proportional to the number of device movements in the Safegraph cohort. The longer arrows with dashed lines represent transits between non-contiguous ZCTAs. The number of device movements ranged from 21139 (corresponding to the transit 11229 → 11235) to 5002 (corresponding to 11214 → 11224). Transits between ZCTAs with fewer than 5,000 movements are not shown. The transits captured by the arrows comprised 44.5% of all device movements between ZCTAs. For base map of New York City ZCTAs, see ref. (33).

estimate $\beta_9 = -0.006$ is no longer significantly different from zero ($p = 0.87$).

Movements within and between regulatory zones

The results of our paired analysis of restaurants and other eating places, as shown in Figure 7, narrowly reflect trips to a specific category of establishments that were subject to specific regulatory controls. They do not necessarily capture broader trends in unregulated movements of individuals within and between zones.

Supplementary Table A1 delineates movements of devices within and between zones, as well as movements outside the regulated area, during the 3 weeks before and the subsequent 3 weeks after the regulations went into effect on October 9. Comparison of the movement matrices during the two time periods (September 18 through October 8, October 9 through October 29) indicates that overall movement patterns remained stable. Among devices homed in the original red zone, only 57–58% of movements were confined to the red zone, while 23–24% of movements were to destinations outside the regulated area entirely. The same pattern is evident in the movements of devices homed in the original orange and yellow zones as well.

The overall stability of within-zone movements seen in Supplementary Table A1 could still obscure significant changes in mobility, particularly in the proportion of devices that made few if any movements. Supplementary Figure A2, however, shows that the percentage of devices that made no movements at all rose only by 1 to 2 percentage points.

Figure 8 tracks more detailed movements between ZCTAs, rather than between regulatory zones, during October 25 through November 28. This time period corresponds to the final 5 weekly maps in Figure 6, when COVID-19 was increasing both in the central ZCTAs and the peripheral ZCTAs along the southern and western edges of the regulated area. The width of each arrow corresponds to the magnitude of the flow between ZCTAs. The figure demonstrates that dominant inter-ZCTA movements were between four red-zone ZCTAs (11229, 11223, 11230, 11204) and three orange- and yellow-zone ZCTAs (11235, 11224, 11214). Moreover, there was significant device traffic between these southern ZCTAs and other peripheral ZCTAs to the west of the regulated area.

Influence of high-risk ZCTAs: Geospatial analysis

Based upon our findings in Figure 8, we identified five high-mobility ZCTAs as potential candidates for high-risk transmission to other surrounding ZCTAs in the area: 11223, 11229, 11235, 11224, and 11214. As seen in Figure 2A, two of the areas, 11224 and 11214, were not in the original red zone,

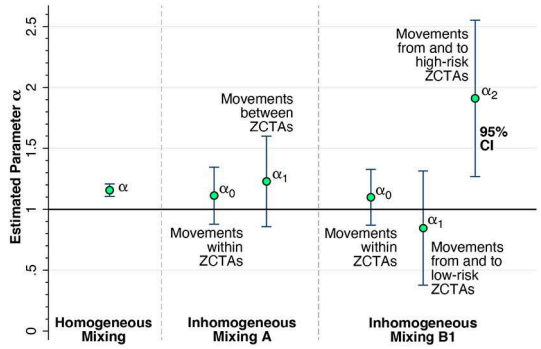

FIGURE 9
Estimates of the reproductive number α from a series of geospatial analyses. **(Left)** Estimate of a uniform parameter $\alpha = 1.157$ with 95% confidence interval [1.106, 1.208] for the entire regulated region, based upon the assumption of homogeneous mixing. The estimate of α is significantly different from 1.0 (2-sided F-test, $p < 0.001$). **(Middle)** Estimates of the parameters α_0 for the effect of movements within ZCTAs and α_1 for between-ZCTA movements, based upon a two-parameter model of inhomogeneous mixing A. **(Right)** Estimates of the parameters α_0 for the effect of movements within ZCTAs, α_1 for the effect of movements from and to low-risk ZCTAs, and α_2 for the effect of movements from and to high-risk ZCTAs 11223, 11229, 11235, 11224, and 11214, based upon a three-parameter model of inhomogeneous mixing B1. The estimated parameter $\alpha_2 = 1.910$ with 95% confidence interval [1.268, 2.552] was significantly different from 1.0 (2-sided F-test, $p = 0.012$). Full details are given in Supplementary Table C1.

while another area, 11235, was excluded from the red zone when the zones were contracted on November 3.

Figure 9 shows the principal results of our geospatial analysis. At the left end of the graphic, in a model of homogeneous mixing with a single, uniform parameter for the entire regulated area (equation 2 in the Methods section), the estimated reproductive number was $\alpha = 1.157$ with 95% confidence interval [1.106, 1.208]. The middle panel shows the results of a two-parameter model of inhomogeneous mixing A, which allowed for movements within ZCTAs to have a different effect on COVID-19 transmission (equation 3). Both parameters α_0 for within-ZCTA movements and α_1 for between-ZCTA movements were in the range of 1.1-—1.2, though they were too imprecise to be distinguishable from each other or from 1.0.

The right-hand panel of Figure 9 shows the estimates of the three-parameter model with inhomogeneous mixing B1 (equation 4), which further distinguished the five high-risk ZCTAs 11223, 11229, 11235, 11224, and 11214 from the remaining sixteen low-risk ZCTAs. The estimate of α_0 was imprecise but consistent with the findings in the two-parameter model A in the middle panel. The estimate of α_1 for low-risk ZCTAs was likewise imprecise, but pointed to a reproductive number <1.0. By contrast, the estimate of α_2 for the effect of device traffic to and from the five high-risk ZCTAs gave a reproductive number of 1.910 with 95% confidence interval [1.268, 2.552]. Moreover, the estimate of α_2 was significantly different from α_0 ($p = 0.045$) and α_1 ($p = 0.012$) based upon 2-sided F-tests.

The alternative test of the three-parameter model with inhomogeneous mixing B2 (equation 4), based upon the classification of all the original red-zone ZCTAs as high risk, did not yield such precise results. The estimate of α_2 for the effect of device traffic to and from these original red-zone ZCTAs gave a reproductive number of 1.485 with 95% confidence interval [0.992, 1.978]. This estimate was not significantly different from α_0 ($p = 0.284$) or from α_1 ($p = 0.124$). The complete results of the geospatial analysis are shown in Supplementary Table C1.

Supplementary Table C2 displays the effects of incorporating three demographic characteristics as covariates in our model: the proportion Hispanic-Latino, the proportion black non-Hispanic, and the proportion receiving public assistance. None of the coefficients of these covariates achieved statistically significance at the 5-percent level. The results were consistent with those reported in Figure 9.

Discussion

Non-identifiability of the effect of the governor's regulatory scheme

Our analysis of paired eating places straddling the red-orange border suggests that the Governor's October 6 regulatory scheme did indeed have some effect. The red-zone rules allowed for only takeout and delivery, while the less stringent orange-zone rules allowed for outdoor dining as well (23). By the week ending November 5, as seen in Figure 7, device visits to establishments on the red side of the red-orange border were down 17.2 percent more than their counterparts on the orange side. Attributing the entire decline to the regulatory scheme is problematic, however, inasmuch as device visits to establishments on the red side of border were already dropping more rapidly during the week ending October 8. Aside from voluntary action on the part of the red zone's residents, the Mayor's threats to impose controls in five key zip codes in South Brooklyn, voiced as early as September 29 (21), may have contributed to a preexisting downward trend.

What's more, a demonstrated narrow effect on a specific endpoint such as restaurant visits does not necessarily imply that the regulatory scheme had an overall deterrent effect on SARS-CoV-2 transmission in South Brooklyn. The COVID-19 incidence data in Figure 4 do show a temporary decline during the weeks ending October 17, 24, and 31, after the regulatory scheme had entered into force. However, as in our interpretation of the restaurant visitation data in Figure 7, COVID-19 incidence was declining during the week before any controls went into effect. And in view of the ∼5-day

incubation period between initial infection and the subsequent development of symptoms warranting testing (46), the incidence of the disease was likely to have been declining even earlier. These considerations reinforce the conclusion that the actual effect of the Governor's regulatory scheme is, strictly speaking, not identifiable from the available data.

Even if the Governor's regulatory scheme was at least partly responsible for retarding the surge of COVID-19 in the central red zone during the last 3 weeks of October, it is evident that the program's success was short-lived. As Figures 4, 6 show, the decline in COVID-19 incidence during October was ultimately reversed by a wave of increasing disease incidence that had similarly overtaken the surrounding orange and yellow zones by the end of November. These observations beg the question: Why did the Governor's scheme ultimately fail?

Overreliance on test positivity

One clue is offered by the striking discordance between the upward surge of disease *incidence* and the continuing downward trend in *test positivity* during the week ending November 9, as shown in Figure 5. The underlying explanation for the discordance of these two trends was the continuing expansion of testing, which diluted the rising incidence with an abundance of negative test results. It was just at this juncture that regulators, overly fixated on the test positivity rate, cut the size of the red zone in half and then converted the red zone to orange. Under this interpretation of the evidence, the Governor's regulatory scheme did have an initial retardant effect on COVID-19 incidence, but subsequent premature withdrawal of regulatory controls neutralized the effect of the initial policy.

Access controls vs. restrictions on population movement

The regulations imposed in the Governor's concentric regulatory zones were fundamentally controls on access – to eating places, to school buildings, to houses of worship, and to large meetings. They differ from the classic remedy of containment, which entails restrictions not just on access, but also on overall population movement (47–49). Although restricting access to some critical locations is indeed likely to reduce disease propagation (15–17, 50, 51), the question here is whether focused controls on access alone were sufficient to alter the underlying population movement patterns that served as the template for a surge in COVID-19 cases. While some have cited increasing indoor activity with the arrival of colder fall weather (52) or a trend toward large family gatherings as the Thanksgiving holiday approached (53), we have in mind more fundamental, well-established contact networks.

The hypothesis that the underlying population movement patterns within the regulated area in South Brooklyn were insufficiently altered by the Governor's regulatory controls on access was supported by the stability of the interzone movement matrices before and after the promulgation of the regulatory scheme (Supplementary Table A1) as well as absence of any significant change in the proportion of devices with no movements (Supplementary Figure A3).

High-movement ZCTAs as drivers of the local COVID-19 surge

One interpretation of the trends in Figure 4 is that the surge in COVID-19 cases that ultimately overran South Brooklyn was a citywide phenomenon, and that the incidence of the disease was simply increasingly uniformly across all ZCTAs. However, the patterns of declining and rising COVID-19 incidence seen in Figure 6 go against this interpretation. Once the incidence reached a low point around the week ending October 17, the subsequent increase was driven by ZCTAs along the southern and western borders of the area. During the resurgence of COVID-19 incidence, movement patterns were hardly uniform, as shown in Figure 8. In fact, the geospatial analysis demonstrates that five high-movement ZCTAs – of which only two were part of the original red zone – were the main drivers of the resurgence in COVID-19, with a reproductive number close to 2, as shown in the panel labeled Inhomogeneous Mixing B1 in Figure 9. That population movement was the critical determinant is further supported by the finding of the inferior performance of Model B2, based upon the Governor's original partitioning of regulatory zones (Supplementary Table C1).

A natural experiment

Our study is fundamentally observational. We did not analyze a macro-experiment in which various communities were randomly assigned to different regulatory controls or no intervention at all (54). Still, our setup has many of the features of a natural experiment. The Governor's announcement of a new regulatory regime on October 6, to become effective by October 9, could reasonably be characterized as an abrupt shock (7). In view of the Mayor's earlier threats to impose controls on certain zip codes in South Brooklyn (21), however, it could hardly be considered an unanticipated shock. The implementation of distinct regulations within each of three concentric regulatory zones provided natural intervention and control groups, and the results of our paired restaurant analysis (Figure 7) suggest that the regulations on access were effective and enforced. While the restaurants stayed put, however, Supplementary Table A1 and Figure 8 show that the experimental participants crossed over from one zone to another. Midway through the intervention, on

November 9, the Governor cut the regulatory zones in half (27), thereby contaminating the original experimental assignments.

Questions of generalizability

Our study has focused on a narrowly defined geographic location during a specific wave of the COVID-19 epidemic. Generalization of the current findings to other settings or other phases of the epidemic needs to proceed with caution. Still, the evidence reported here is broadly consistent with findings reported in Hong Kong (8), in Shenzhen, China (18), in Dublin, Ireland (13), in Cataluña, Spain (16), in various Latin American cities (9), and in other sites in Asia Pacific and Europe (20). The critical role of mobility has also been demonstrated in the most populous counties of the United States during the Omicron variant wave of the COVID-19 epidemic during December 2021 –February 2022 (14).

Conclusions

Combining data on COVID-19 incidence and testing outcomes with data on the movements of devices equipped with location-tracking software, we found that a regulatory scheme of concentric geographic zones imposing graduated restrictions on access did not halt the surge of COVID-19 in South Brooklyn, New York, during October-November 2020.

Beyond this principal conclusion, we can reasonably draw some additional inferences from the accumulated evidence. First, test positivity as a real-time indicator of regulatory effectiveness is fraught with potential biases (55, 56). Here, the Governor and his advisors may have been led astray by a test positivity rate that was kept misleadingly close to three percent by an endogenous increase in testing among COVID-negative persons (Figure 5).

Second, while restrictions on access to eating establishments and other high-risk venues may be narrowly effective (Figure 7), they do not prevent people from moving around (Supplementary Table A1 and Figure 8). In highly populous areas such as South Brooklyn, a halfway strategy of concentric regulatory zones based solely on access restrictions may be no substitute for the classic approach of concentric containment/quarantine areas (6, 49).

Third, overreliance on static rather than dynamic measures of disease burden to draw the boundaries of regulatory zones can prove to be highly misleading. Our geospatial analysis of COVID-19 incidence, entailing a dynamic model of COVID-19 incidence across 21 zip code tabulation areas (Figure 9), identified five high-movement ZCTAs where the reproductive number approached 2. Two of the five were not in the original red zone. Concentric zones may appear to be an effective regulatory approach in principle, but only if the boundaries are drawn correctly.

Fourth, policies restricting movement can take many forms, including controls on transportation networks. There is substantial evidence pointing to the initial widespread dissemination of SARS-CoV-2 *via* New York City's subway-based network during February-March 2020, followed by percolation of new infections within local community hotspots (57). A policy of running express lines with limited density might have been an alternative to the complete shutdown of subway lines adopted in Wuhan (58).

Finally, in extreme cases, it may be necessary to impose stay-at-home restrictions. During an outbreak in September 2020 on the campus of the University of Wisconsin-Madison, the university administration barred students from leaving two highly infected residence halls. By the end of the month, COVID-19 incidence on campus had fallen below that of the surrounding county (51). Even so, such stay-at-home orders may prove incompletely effective when disease propagation is dominated by intrahousehold transmission, as it was during the winter COVID-19 surge in Los Angeles County, a region with a high prevalence of multi-generational households (59). Whether such a stay-at-home order would have been effective or even feasible in the case of South Brooklyn remains an open question.

Data availability statement

Publicly available datasets were analyzed in this study. This data can be found here: Supporting programs and data have been posted at the Open Science Framework https://osf.io/rquyx/.

Author contributions

JH is the sole author of this work. He is responsible for the conceptualization of the study, the data analysis, the drafting of the manuscript, and the creation of the figures.

Conflict of interest

The author declares that the research was conducted in the absence of any commercial or financial relationships that could be construed as a potential conflict of interest.

Publisher's note

All claims expressed in this article are solely those of the authors and do not necessarily represent those

of their affiliated organizations, or those of the publisher, the editors and the reviewers. Any product that may be evaluated in this article, or claim that may be made by its manufacturer, is not guaranteed or endorsed by the publisher.

Supplementary material

The Supplementary Material for this article can be found online at: https://www.frontiersin.org/articles/10.3389/fpubh.2022.970363/full#supplementary-material

References

1. U.S. Department of Agriculture. *Develop a Surveillance Plan: Disease Control Areas / Zones*. (2020). Available online at: https://www.aphis.usda.gov/aphis/ourfocus/animalhealth/ceah-toolbox/section-3.-disease-control-areas-and-zones: Animal and Plant Health Inspection Service, Updated June 2.

2. Department of the Interior and Local Government (DILG), *RIATF-RTF NCR lead zoning containment strategy orientation*. (2020). Available online at: http://ncr.dilg.gov.ph/home/riatf-rtf-ncr-leads-zoning-containment-strategy-orientation/: Republic of the Philippines.

3. Gotinga, J.C. *Zonal lockdowns: Is your house, street, or city a critical zone*? (2020). Available online at: https://www.rappler.com/newsbreak/iq/explainer-zonal-coronavirus-lockdowns

4. Bajardi P, Poletto C, Ramasco JJ, Tizzoni M, Colizza V, Vespignani A. Human mobility networks, travel restrictions, and the global spread of 2009 H1N1 pandemic. *PLoS ONE*. (2011) 6:e16591. doi: 10.1371/journal.pone.0016591

5. Rea E, Lafleche J, Stalker S, Guarda BK, Shapiro H, Johnson I, et al. Duration and distance of exposure are important predictors of transmission among community contacts of Ontario SARS cases. *Epidemiol Infect*. (2007) 135:914–21. doi: 10.1017/S0950268806007771

6. Kuo FY, Wen TH. Regionalization for infection control: an algorithm for delineating containment zones considering the regularity of human mobility. *Appl Geogr*. (2021) 126:102375. doi: 10.1016/j.apgeog.2020.102375

7. New York Governor, *Governor Cuomo Announces New Cluster Action Initiative*. (2020). Available online at: https://www.governor.ny.gov/news/governor-cuomo-announces-new-cluster-action-initiative

8. Wong PP, Low CT, Lai PC. The impact of geographic mobility on the spread of COVID-19 in Hong Kong. *Geospat Health*. (2022) 17:1022. doi: 10.4081/gh.2022.1022

9. Kephart JL, Delclòs-Alió X, Rodríguez DA, Sarmiento OL, Barrientos-Gutiérrez T, Ramirez-Zea M, et al. The effect of population mobility on COVID-19 incidence in 314 Latin American cities: a longitudinal ecological study with mobile phone location data. *Lancet Digit Health*. (2021). 3:e716–722. doi: 10.1016/S2589-7500(21)00174-6

10. Oh J, Lee HY, Khuong QL, Markuns JF, Bullen C, Barrios OE, et al. Mobility restrictions were associated with reductions in COVID-19 incidence early in the pandemic: evidence from a real-time evaluation in 34 countries. *Sci Rep*. (2021) 11:13717. doi: 10.1038/s41598-021-92766-z

11. Nouvellet P, Bhatia S, Cori A, Ainslie KE, Baguelin M, Bhatt S, et al. Reduction in mobility and COVID-19 transmission. *Nat Commun*. (2021) 12:1090. doi: 10.1038/s41467-021-21358-2

12. He S, Lee J, Langworthy B, Xin J, James P, Yang Y, et al. Delay in the effect of restricting community mobility on the spread of COVID-19 during the first wave in the United States. *Open Forum Infect Dis*. (2022) 9:ofab586. doi: 10.1093/ofid/ofab586

13. Manzira CK, Caulfield B. Assessing the impact of mobility on the incidence of COVID-19 in Dublin City. *Sustain Cities Soc*. (2022) 80:103770. doi: 10.1016/j.scs.2022.103770

14. Harris JE. Mobility was a significant determinant of reported COVID-19 incidence during the Omicron surge in the most populous U.S. counties. *BMC Infect Dis*. (2022) 22:691. doi: 10.1186/s12879-022-07666-y

15. Schnake-Mahl AS, O'Leary G, Mullachery PH, Vaidya V, Connor G, Rollins H, et al. The impact of keeping indoor dining closed on COVID-19 rates among large US cities: a quasi-experimental design. *Epidemiology*. (2022) 33:200–8. doi: 10.1097/EDE.0000000000001444

16. Leon. Evaluating the policy of closing bars and restaurants in Cataluna and its effects on mobility and COVID19 incidence. *Sci Rep*. (2022) 12:9132. doi: 10.1101/2020.04.21.20073049

17. Brauner JM, Mindermann S, Sharma M, Johnston D, Salvatier J, Gavenčiak T, et al. Inferring the effectiveness of government interventions against COVID-19. *Science*. (2021) 371:9338. doi: 10.1126/science.abd9338

18. Zhou Y, Xu R, Hu D, Yue Y, Li Q, Xia J. Effects of human mobility restrictions on the spread of COVID-19 in Shenzhen, China: a modelling study using mobile phone data. Lancet Digit Health. (2020). 2(8): p. e417–e424. doi: 10.1016/S2589-7500(20)30165-5

19. Chinazzi M, Davis JT, Ajelli M, Gioannini C, Litvinova M, Merler S, et al. The effect of travel restrictions on the spread of the 2019 novel coronavirus (COVID-19) outbreak. *Science*. (2020) 368:395–400. doi: 10.1126/science.aba9757

20. Han E, Tan MM, Turk E, Sridhar D, Leung GM, Shibuya K, et al. Lessons learnt from easing COVID-19 restrictions: an analysis of countries and regions in Asia Pacific and Europe. *Lancet*. (2020) 396:1525–34. doi: 10.1016/S0140-6736(20)32007-9

21. Lardieri A. *De Blasio Warns of Reimposing Coronavirus Restrictions as New York Positivity Rate Rises*. (2020). Available online at: https://www.usnews.com/news/health-news/articles/2020-09-29/de-blasio-warns-of-reimposing-coronavirus-restrictions-as-new-york-positivity-rate-rises

22. Kim E, Pereira S. *De Blasio Moves To Order Shutdowns In 9 Brooklyn And Queens ZIP Codes With Virus Outbreaks*. (2020). Available online at: https://gothamist.com/news/nyc-moves-order-shutdowns-9-brooklyn-and-queens-zip-codes-virus-outbreaks

23. New York Governor, *New York "Micro-Cluster" Strategy*. (2020). Available online at: https://www.governor.ny.gov/sites/default/files/atoms/files/MicroCluster_Metrics_10.21.20_FINAL.pdf

24. New York Governor. *Governor Cuomo Details COVID-19 Micro-Cluster Metrics*. (2020). Available online at: https://www.governor.ny.gov/news/governor-cuomo-details-covid-19-micro-cluster-metrics

25. U.S. Supreme Court. *Roman Catholic Diocese of Brooklyn, New York v. Andrew M. Cuomo, Governor of New York*. (2020). Available online at: https://www.supremecourt.gov/opinions/20pdf/20a87_4g15.pdf

26. New York Governor. *Governor Cuomo Announces State Will Withhold Funds for Localities and Schools in COVID-19 Cluster Zones That Fail to Enforce Public Health Law*. (2020). Available online at: https://www.governor.ny.gov/news/governor-cuomo-announces-state-will-withhold-funds-localities-and-schools-covid-19-cluster

27. New York Governor, *Governor Cuomo Announces Updated COVID-19 Micro-Cluster Focus Zones*. (2020). Available online at: https://www.governor.ny.gov/news/governor-cuomo-announces-updated-covid-19-micro-cluster-focus-zones

28. New York Governor. *Governor Cuomo Announces Updated COVID-19 Micro-Cluster Focus Zone*. (2020). Available online at: https://www.governor.ny.gov/news/governor-cuomo-announces-updated-covid-19-micro-cluster-focus-zones-2

29. New York Governor. *Brooklyn Large Map*. (2020). Available online at: https://www.governor.ny.gov/sites/default/files/atoms/files/Brooklyn_large_map.pdf

30. New York Governor. *Brooklyn_HiRes2.pdf (Map)*. (2020). Available online at: https://www.governor.ny.gov/sites/default/files/atoms/files/Brooklyn_HiRes2.pdf: October 21.

31. New York Governor. *Brooklyn_New_Zones_11_03_2020 (Map)*. (2020). Available online at: https://www.governor.ny.gov/sites/default/files/atoms/files/Brooklyn_New_Zones_11_03_2020.pdf

32. New York Governor. *Brooklyn New Zones (Map)*. (2020). Available online at: https://www.governor.ny.gov/sites/default/files/atoms/files/Brooklyn_New_Zones_11_03_2020.pdf

33. New York City Department of Health and Mental Hygiene. *Geo Files*. (2022). Available online at: https://github.com/nychealth/coronavirus-data/tree/master/Geography-resources (accessed April 27).

34. SafeGraph Inc. *Social Distancing Metrics*. (2020). Available online at: https://docs.safegraph.com/docs/social-distancing-metrics

35. QGIS Development Team. *QGIS Geographic Information System*. (2021). Available online at: http://qgis.osgeo.org

36. U.S Census Bureau. *TIGER2017 Shape Files for Census Block Groups by State*. (2017). Available online at: https://www2.census.gov/geo/tiger/TIGER2017/BG

37. Picard R. *GEOINPOLY: Stata module to match geographic locations to shapefile polygons*. (2015). Available online at: https://ideas.repec.org/c/boc/bocode/s458016.html

38. SafeGraph Inc. *Places Schema*. (2020). Available online at: https://docs.safegraph.com/docs/places-schema (accessed July 30–31, September 24–26).

39. U.S Census Bureau. TIGER/Line Shapefile. State, New York, Current Block Group State-based (2021). Available online at: https://catalog.data.gov/dataset/tiger-line-shapefile-2017-state-new-york-current-block-group-state-based

40. New York City Department of Health and Mental Hygiene, caserate-by-modzcta.csv (Weeks ending 8/8 through 11/28/2020). (2020). Available online at: https://raw.githubusercontent.com/nychealth/coronavirus-data/84dead220def7b53bcb2d9f9210609dee9446045/trends/caserate-by-modzcta.csv

41. New York City Department of Health and Mental Hygiene, *percentpositive-by-modzcta.csv*. (2021). Available online at: https://github.com/nychealth/coronavirus-data/blob/master/trends/percentpositive-by-modzcta.csv

42. Picard R. GEONEAR: Stata module to find nearest neighbors using geodetic distances. (2019). Available online at: https://ideas.repec.org/c/boc/bocode/s457146.html

43. Kolokolnikov T, Iron D. Law of mass action and saturation in SIR model with application to Coronavirus modelling. *Infect Dis Model.* (2021) 6:91–7. doi: 10.1016/j.idm.2020.11.002

44. Vogels EA. Digital divide persists even as Americans with lower incomes make gains in tech adoption. (2021). Available online at: https://www.pewresearch.org/fact-tank/2021/06/22/digital-divide-persists-even-as-americans-with-lower-incomes-make-gains-in-tech-adoption/

45. Anderson M. Racial and ethnic differences in how people use mobile technology. (2015). Available online at: https://www.pewresearch.org/fact-tank/2015/04/30/racial-and-ethnic-differences-in-how-people-use-mobile-technology/

46. Lauer SA, Grantz KH, Bi Q, Jones FK, Zheng Q, Meredith HR, et al. The incubation period of coronavirus disease 2019 (COVID-19) from publicly reported confirmed cases: estimation and application. *Ann Intern Med*. (2020) 172:577–82. doi: 10.7326/M20-0504

47. Chiew. Can we contain the COVID-19 outbreak with the same measures as for SARS? *Lancet Infect Dis*. (2020) 20:e102–7. doi: 10.1016/S1473-3099(20)30129-8

48. Day T, Park A, Madras N, Gumel A, Wu J. When is quarantine a useful control strategy for emerging infectious diseases? *Am J Epidemiol*. (2006) 163:479–85. doi: 10.1093/aje/kwj056

49. Yacoub. The concept of quarantine in history: from plague to SARS. *J Infect*. (2004) 49:257–61. doi: 10.1016/j.jinf.2004.03.002

50. Harris JE. COVID-19, bar crowding, and the Wisconsin supreme court: a non-linear tale of two counties. *Res Int Bus Finance*. (2020) 54:101310. doi: 10.1016/j.ribaf.2020.101310

51. Harris JE. Geospatial analysis of a COVID-19 outbreak at the university of Wisconsin - Madison: potential role of a cluster of local bars. *Epidemiol Infect*. (2022) 3:1–31. doi: 10.1017/S0950268822000498

52. Mallapaty S. Why COVID outbreaks look set to worsen this winter. *Nature*. (2020) 586:653. doi: 10.1038/d41586-020-02972-4

53. Mehta SH, Clipman SJ, Wesolowski A, Solomon SS. Holiday gatherings, mobility and SARS-CoV-2 transmission: results from 10 US states following. *Thanksgiving Sci Rep*. (2021) 11:17328. doi: 10.1038/s41598-021-96779-6

54. Harris JE. Macro-experiments versus micro-experiments for health policy, in *Social Experimentation*, Wise JH editor, Chicago: University of Chicago Press (1985). Available online at: https://www.nber.org/books-and-chapters/social-experimentation/macroexperiments-versus-microexperiments-health-policy. p. 145-186.

55. Harris JE. *Reopening Under COVID-19: What to Watch For*. (2020). Available online at: http://web.mit.edu/jeffrey/harris/HarrisJE_WP3_COVID19_WWF_6-May-2020.pdf. doi: 10.3386/w27166

56. Harris JE. *The Test Positivity Rate is (Nearly) Useless*. (2020). Available online at: https://lifeunderquarantine.blog/2020/12/04/the-test-positivity-rate-is-nearly-useless/

57. Harris JE. Critical role of the subways in the initial spread of SARS-CoV-2 in New York City. *Front Public Health*. (2021) 9:754767. doi: 10.3389/fpubh.2021.754767

58. BC News. *Coronavirus: Wuhan shuts public transport over outbreak*. (2020). Available online at: https://www.bbc.com/news/world-asia-china-51215348

59. Harris JE. Los Angeles county SARS-CoV-2 epidemic: critical role of multi-generational intra-household transmission. *J Bioecon*. (2021) 23:55–83. doi: 10.1007/s10818-021-09310-2